Research Article | Vol. 28, No. 21 / 12 October 2020 / Optics Express 30656

Optics EXPRESS

Nonlinear dynamics of miniature optoelectronic oscillators based on whispering-gallery mode electrooptical modulators

HELENE NGUEWOU-HYOUSSE AND YANNE K. CHEMBO*

University of Maryland, Department of Electrical and Computer Engineering & Institute for Research in Electronics and Applied Physics (IREAP), 8279 Paint Branch Dr, College Park MD 20742, USA
ykchembo@umd.edu

Abstract: We propose a time-domain model to analyze the dynamical behavior of miniature optoelectronic oscillators (OEOs) based on whispering-gallery mode resonators. In these systems, the whispering-gallery mode resonator features a quadratic nonlinearity and operates as an electrooptical modulator, thereby eliminating the need for an integrated Mach-Zehnder modulator. The narrow optical resonances also eliminate the need for both an optical fiber delay line and an electric bandpass filter in the optoelectronic feedback loop. The architecture of miniature OEOs therefore appears as significantly simpler than the one of their traditional counterparts and permits us to achieve competitive metrics in terms of size, weight, and power. Our theoretical approach is based on the closed-loop coupling between the optical intracavity modes and the microwave signal generated via the photodetection of the output electrooptical comb. The resulting nonlinear oscillator model involves the slowly-varying envelopes of the microwave and optical fields, and its stability analysis permits the analytical determination the critical value of the feedback gain needed to trigger self-sustained oscillations. This stability analysis also allows us to understand how key parameters of the system such as cavity detuning or coupling efficiency influence the onset of the radiofrequency oscillation. Our study is complemented by time-domain simulations for the microwave and optical signals, which are in excellent agreement with the analytical predictions.

1. Introduction

Optoelectronic oscillators (OEOs) are microwave photonic systems that concatenate a optical and electronic branch in a closed feedback loop. They have found numerous applications in lightwave and microwave technology, such as in communication engineering, sensing, analog computing, and most importantly, time-frequency metrology (see review article [1]). Indeed, one of the most noteworthy application of OEOs is ultra-low phase noise radiofrequency generation. This outcome can achieved via the combination of photon storage in a long optical delay line and narrowband electric filtering, as initially proposed by Yao and Maleki [2–4].

In its most conventional configuration, the OEO for ultrapure microwave generation incorporates a laser, an electrooptical (EO) Mach-Zehnder modulator, a few-km-long optical delay line, a photodiode, an electrical bandpass filter and an RF amplifier, as shown in Fig. 1(a). Using these commercial-off-the-shelf (COTS) components permits to achieve remarkable phase noise performances, down to a record −163 dBc/Hz at 6 kHz offset from a 10 GHz carrier [5]. However, the main drawback of these architectures is that they are bulky, heavy, and energy-greedy – thus not satisfying the fundamental constraints of size, weight and power (SWAP).

Several alternatives approaches have been proposed to ensure SWAP convergence for OEOs. One of the most promising approach has been to replace both the delay-lines and electric bandpass filters with whispering-gallery mode (WGM) resonators, which are low-loss dielectric cavities capable of trapping photons for long durations via total internal reflection [6–11]. The lifetime τ_{ph}

#404791 https://doi.org/10.1364/OE.404791
Journal © 2020 Received 7 Aug 2020; revised 14 Sep 2020; accepted 17 Sep 2020; published 29 Sep 2020

Optics EXPRESS

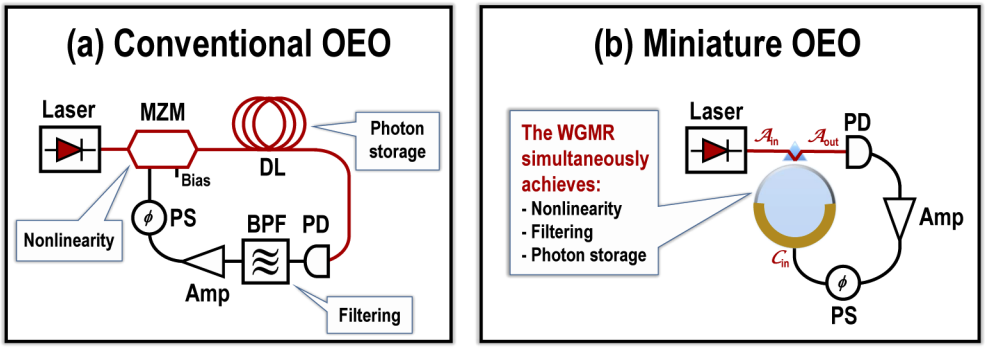

Fig. 1. Comparison between the architectures of conventional and miniature OEOs. The optical paths are in red, and the electric paths in black. Polarization controllers between the lasers and the modulators are generally necessary, but have been omitted here for the sake of simplicity. (a) Conventional OEO. MZM: Mach-Zehnder modulator; DL: Delay line; PD: Photodiode; PS: Phase shifter; BPF: Narrowband bandpass filter; Amp: RF amplifier. (b) Miniature OEO. WGMR: Whispering-gallery mode resonator; The other acronyms are the same as in (a). Note that in the miniature OEO, the WGMR is a single component that replaces the MZM, the DL and the BPF in the conventional OEO.

of an intracavity photon of angular frequency ω_0 characterizes the optical storage capability of the resonator, and is linked to its quality factor following $Q = \omega_0 \tau_{\mathrm{ph}}$. At the telecom wavelength of 1550 nm, the photon lifetime in ultra-high-Q WGM resonators can typically vary from few tenths to few tens of μs; equivalently, the loaded linewidth $2\kappa = 1/\tau_{\mathrm{ph}}$ of the corresponding resonances varies from few tens to few tenths of MHz ($\times 2\pi$). Therefore, because they could perform both photon storage and narrowband filtering in the *linear* regime, millimetric or sub-millimetric WGM resonators have been successfully inserted on OEO loops, and they have permitted a significant reduction of the oscillators in terms of size – see for example Refs. [12–21].

An additional step can be considered in order to accelerate the SWAP convergence: it is to couple a microwave strip cavity to a WGM resonator with $\chi^{(2)}$ nonlinearity, which can then play the role of an electrooptical modulator and eliminate the need for its Mach-Zehnder equivalent [22]. In this case, the three tasks of photon storage, narrowband filtering and nonlinearity can be performed by the WGM resonator: the oscillator therefore becomes a *miniature OEO*, whose architecture is displayed in Fig. 1(b). As discussed by Maleki in Ref. [23], the main interest of this approach is that it effectively leads to the best SWAP performance for OEOs.

At this date, the deterministic dynamics of narrowband OEOs with time-delayed feedback is quite well understood, and it is based on the approach of microwave envelope equations [1]. However, to the best of our knowledge, there is no theoretical model available to analyze the nonlinear dynamics and stability of miniature OEOs. Indeed, understanding the dynamical behavior of miniature OEOs requires an analysis of the electrooptical conversion phenomena that are taking place in a WGM cavity pumped by both a resonant laser and coupled to a RF strip cavity pumped by a microwave signal. These intracavity processes, which involve microwave and optical photons interacting quantum-mechanically, are the fundamental phenomena enabling the concepts of electrooptical WGM modulators [24–28] and ultra-sensitive microwave photonic receivers [29–37] .

Most works related to electrooptical WGM resonators are restricted to the three-modes operation involving the pump, signal and idler modes. A noteworthy exception is for example the work of Ilchenko *et al.* in Ref. [28], where they analyzed the intracavity dynamics for an arbitrary number of modes. The multimode analysis is indispensable for the understanding and characterization of the miniature OEO, as these cascaded intracavity interactions contribute to

Optics EXPRESS

the saturation nonlinearity in the feedback loop, thereby defining the amplitude of the stationary microwave and lightwave oscillations.

The objective of this article is therefore to propose a full time-domain model accounting for all nonlinear interactions in miniature OEOs based on electrooptical WGM modulators. We also aim at performing an analytical stability study that will permit the determination of the threshold value of the feedback gain beyond which self-starting oscillations are triggered.

This article is organized as follows. Section 2 is devoted to the description of the miniature OEO under study. The time-domain equations governing the dynamics of the microwave and optical intracavity fields in the open-loop configuration – corresponding to the multimode model for the electrooptical modulator – are presented in Sec. 3, where the semiclassical equations are subsequently deduced from their quantum counterparts. The closed-loop equations ruling the dynamics of the miniature OEO are derived in Sec. 4, where a stability analysis is performed to determine the threshold gain for the self-oscillations. The optimization analysis is led in Sec. 5, while Sec. 6 analyzes the important case of amplifierless miniature OEOs. The last section concludes the article.

2. System

The miniature OEO under study is displayed in Fig. 1(b). The WGM resonator is a lithium niobate (LN) disk of main radius a, that is used as a resonant electrooptical modulator. This modulator has an optical input, an RF input, and an optical output. The optical input is a telecom laser signal at power P_{L} with wavelength $\lambda_{\mathrm{L}} \simeq 1550$ nm, and the corresponding angular frequency is $\omega_{\mathrm{L}} = 2\pi c/\lambda_{\mathrm{L}}$ with c being the velocity of light in vacuum. The WGM resonator has a free-spectral range that can be determined as $\Omega_{\mathrm{R}} = c/an_{\mathrm{g}} = 2\pi/T_{\mathrm{R}}$, where n_{g} is the group velocity index of the lithum niobate at the pump wavelength, and T_{R} is the photon round-trip time in the optical cavity.

The WGM cavity has a loaded quality factor $Q = \omega_{\mathrm{L}}/2\kappa$, where $\kappa = \kappa_{\mathrm{i}} + \kappa_{\mathrm{e}}$ is the loaded half-linewidth of the resonances at telecom wavelength, while $\kappa_{\mathrm{i}} = \omega_{\mathrm{L}}/2Q_{\mathrm{i}}$ and $\kappa_{\mathrm{e}} = \omega_{\mathrm{L}}/2Q_{\mathrm{e}}$ correspond to the intrinsic and extrinsic (i.e., coupling) contributions, respectively [10].

The WGMs of the resonator that are involved in this process belong to the same mode family. Therefore, they can be unambiguously labelled by their azimuthal order ℓ. Since the pumped mode has an azimuthal order ℓ_0, it is useful to introduce the reduced azimuthal order $l = \ell - \ell_0$ so that the WGMs involved in the system's dynamics can now be symmetrically labeled as $l = 0, \pm 1, \pm 2, \ldots$, with $l = 0$ being the pumped mode which has a resonant frequency ω_0. The pump frequency ω_{L} is very close to the resonant frequency ω_0 of the pumped mode, the detuning being equal to $\sigma_{\mathrm{A}} = \omega_{\mathrm{L}} - \omega_0$. It is convenient to introduce the normalized optical detuning $\alpha = -\sigma_{\mathrm{A}}/\kappa$, which is such that resonant pumping translates to $|\alpha| \leq 1$.

The RF strip resonator coupled to the WGM disk has a resonance frequency that matches the FSR of the optical cavity. It has a loaded quality factor $Q_{\mathrm{M}} = \Omega_{\mathrm{R}}/2\mu$, where μ is the half-linewidth of the loaded RF cavity resonance. The microwave input with power P_{M} has a frequency Ω_{M} very close to Ω_{R}, with the RF detuning $\sigma_{\mathrm{C}} = \Omega_{\mathrm{M}} - \Omega_{\mathrm{R}}$. Here also, we define the normalized RF detuning $\xi = -\sigma_{\mathrm{C}}/\mu$, which is within the resonance when $|\xi| \leq 1$.

The second-order susceptibility $\chi^{(2)}$ of the lithium niobate crystal is a nonlinearity that mediates the coherent interaction between the microwave photons $\hbar\Omega_{\mathrm{M}}$ fed to the RF strip cavity and the optical photons $\hbar\omega_l$ circulating inside the WGM cavity. At the photon level, the intensity of this nonlinear interaction is weighted by a normalized coupling parameter $g \propto \chi^{(2)}$, which has the dimension of an angular frequency [28,33,37,38]. Interestingly, the ratio between the energy of the optical photons comparatively to their microwave counterparts is approximately equal to their azimuthal eigenumber $\ell \simeq \omega_l/\Omega_{\mathrm{R}}$, which would be here of the order of a few thousands.

The output optical signal of the WGM resonator is an electrooptical frequency comb whose intermodal frequency is an RF signal corresponding to the FSR of the cavity. This comb is sent to

Optics EXPRESS

a photodetector (with sensitivity S), that retrieves this beating intermodal frequency and outputs a microwave signal, which is subsequently amplified and eventually phase shifted before being fed back to the RF electrode of the WGM electrooptical modulator (input impedance R_{out}) – thereby closing the optoelectronic feedback loop. The two main tasks to undertake are now *(i)* to build a time-domain model to describe the dynamics of this oscillator, and *(ii)* to perform the stability analysis of this model in order to determine the threshold gain leading to the self-oscillatory behavior.

Unless otherwise stated, we will consider the following parameters for our system throughout this article, without loss of generality: $P_{\text{L}} = 1$ mW; $\lambda_{\text{L}} = 1550$ nm; $\Omega_{\text{R}}/2\pi = 10$ GHz; $S = 20$ V/W; $g/2\pi = 20$ Hz; $Q_{\text{i}} = 5 \times 10^7$ and $Q_{\text{e}} = 10^7$ (this defines all the κ coefficients); $Q_{\text{M}} = \Omega_{\text{R}}/2\mu = 100$; and finally, the RF line is impedance-matched with the modulator input electrode with $R_{\text{out}} = 50\ \Omega$ and $\mu_{\text{i}} = \mu_{\text{e}} = \mu/2$.

3. Open-loop configuration

The analysis of the open-loop system is an unavoidable preliminary to the study of its closed-loop counterpart. In particular, it is essential for the understanding of the nonlinear dynamics of the WGM electrooptical modulator, which is central to the operation of the miniature OEO.

3.1. Quantum formalism

The interactions inside the WGM generator involve microwave photons of energy $\hbar\Omega_{\text{R}}$, and and optical photons of energy $\hbar\omega_l$. As explained in Fig. 2, the second-order susceptibility $\chi^{(2)}$ mediates two different processes in the resonator. The first one is parametric upconversion following $\hbar\omega_l + \hbar\Omega_{\text{R}} \rightarrow \hbar\omega_{l+1}$. This interaction is always stimulated, i. e., it can only occur when the WGMR is RF-pumped. The second process is parametric downconversion, following $\hbar\omega_l \rightarrow \hbar\omega_{l-1} + \hbar\Omega_{\text{R}}$. This downconversion can be either stimulated (does only occur in presence of RF pumping) or spontaneous (does always occur regardless of RF pumping), with both processes having different microwave photon production rates.

The interaction between optical and microwave photons is best decribed from the quantum-mechanical view point. In that framework, the intracavity fields are described by the annihilation operators $\hat{a}_l$ for the optical modes and $\hat{c}$ for the microwave field, as well as by the corresponding

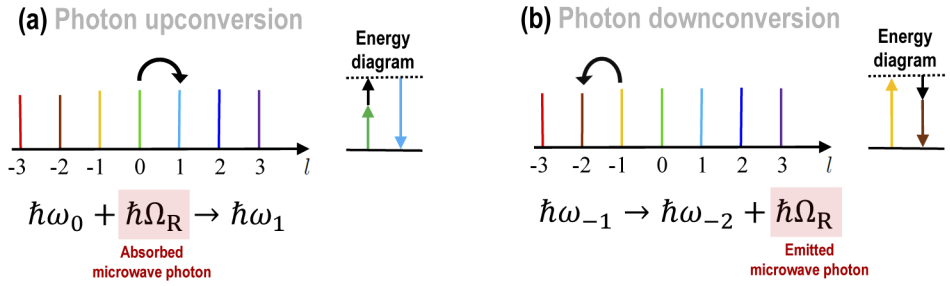

Fig. 2. Frequency-domain representation of photonic up- and down-conversion in a WGM resonator with $\chi^{(2)}$ nonlinearity. These two processes can be leveraged to translate microwave energy to the optical domain inside the WGM resonator. When belonging to the same family, the eigenmodes of the resonator with free-spectral range Ω_{R} are quasi-equidistantly spaced as $\omega_l \simeq \omega_0 + l\Omega_{\text{R}}$, where $l = \ell - \ell_0$ is the reduced azimuthal eigenumber, and ω_0 is the pumped resonance. (a) Photonic upconversion (stimulated): An infrared photon annihilates a microwave photon and is upconverted as $\hbar\omega_l + \hbar\Omega_{\text{R}} \rightarrow \hbar\omega_{l+1}$. (b) Photonic downconversion (stimulated or spontaneous): An infrared photon emits a microwave photon and is downconverted as $\hbar\omega_l \rightarrow \hbar\omega_{l-1} + \hbar\Omega_{\text{R}}$.

Optics EXPRESS

creation operators $\hat{a}_l^\dagger$ and $\hat{c}^\dagger$. All these operators commute, except $[\hat{a}_l, \hat{a}_l^\dagger] = 1$ and $[\hat{c}, \hat{c}^\dagger] = 1$. The operators $\hat{n}_l = \hat{a}_l^\dagger \hat{a}_l$ and $\hat{n}_C = \hat{c}^\dagger \hat{c}$ stand for the photon numbers in the optical and microwave fields, respectively. The optical and microwave input signals are treated as quantum coherent states [39].

The total Hamiltonian of the open-loop system can be explicitly defined as

$$\hat{H}_{\text{tot}} = \hat{H}_{\text{int}} + \hat{H}_{\text{free}} + \hat{H}_{\text{pump}} \tag{1}$$

where

$$\hat{H}_{\text{int}} = \hbar g \sum_m \left\{ \hat{c}\, \hat{a}_m \hat{a}_{m+1}^\dagger + \hat{c}^\dagger \hat{a}_m^\dagger \hat{a}_{m+1} \right\} \tag{2}$$

is the interaction Hamiltonian corresponding to the quadratic nonlinearity of the WGM resonator,

$$\hat{H}_{\text{free}} = \hbar \sigma_{\text{C}}\, \hat{c}^\dagger \hat{c} + \hbar \sigma_{\text{A}} \sum_m \hat{a}_m^\dagger \hat{a}_m \tag{3}$$

is the free Hamiltonian corresponding to the cavity frequency detunings, and

$$\hat{H}_{\text{pump}} = i\hbar\sqrt{2\kappa_{\text{e}}}(\mathcal{A}_{\text{in}} \hat{a}_0^\dagger - \mathcal{A}_{\text{in}}^* \hat{a}_0) + i\hbar\sqrt{2\mu_{\text{e}}}(C_{\text{in}} \hat{c}^\dagger - C_{\text{in}}^* \hat{c})\,, \tag{4}$$

is the Hamiltonian that accounts for the optical and microwave pump fields A_{in} and C_{in}, which are defined as

$$\mathcal{A}_{\text{in}} = \sqrt{\frac{P_{\text{L}}}{\hbar \omega_{\text{L}}}} \quad \text{and} \quad C_{\text{in}} = \sqrt{\frac{P_{\text{M}}}{\hbar \Omega_{\text{M}}}}\,. \tag{5}$$

We can now use the total Hamiltonian $\hat{H}_{\text{tot}}$ to obtain the following equations for the annihilation operators in the Heisenberg picture:

$$\begin{aligned} \dot{\hat{a}}_l &= \frac{1}{i\hbar}[\hat{a}_l, \hat{H}_{\text{tot}}] + \sum_{\text{s=i,e}} \left\{ -\kappa_{\text{s}} \hat{a}_l + \sqrt{2\kappa_{\text{s}}}\, \hat{V}_{\text{s},l} \right\} \\ &= -\kappa(1 + i\alpha)\hat{a}_l - ig(\hat{c}\hat{a}_{l-1} + \hat{c}^\dagger \hat{a}_{l+1}) + \delta(l)\sqrt{2\kappa_{\text{e}}}\, \mathcal{A}_{\text{in}} + \sqrt{2\kappa_{\text{i}}}\, \hat{V}_{\text{i},l} + \sqrt{2\kappa_{\text{e}}}\, \hat{V}_{\text{e},l} \end{aligned} \tag{6}$$

$$\begin{aligned} \dot{\hat{c}} &= \frac{1}{i\hbar}[\hat{c}, \hat{H}_{\text{tot}}] + \sum_{\text{s=i,e}} \left\{ -\mu_{\text{s}} \hat{c} + \sqrt{2\mu_{\text{s}}}\, \hat{W}_{\text{s}} \right\} \\ &= -\mu(1 + i\xi)\hat{c} - ig \sum_m \hat{a}_m^\dagger \hat{a}_{m+1} + \sqrt{2\mu_{\text{e}}}\, C_{\text{in}} + \sqrt{2\mu_{\text{i}}}\, \hat{W}_{\text{i}} + \sqrt{2\mu_{\text{e}}}\, \hat{W}_{\text{e}}\,, \end{aligned} \tag{7}$$

where the temporal vacuum fluctuations associated with losses have been explicitly introduced using the operators $\hat{V}_{\text{i},l}$ ($\hat{V}_{\text{e},l}$) for the intrinsic (extrinsic) optical losses for the mode l, and $\hat{W}_{\text{i}}$ ($\hat{W}_{\text{e}}$) for the intrinsic (extrinsic) microwave losses, respectively. These operators have zero expectation value and obey the commutation rules $[\hat{V}_{\text{s},l}(t), \hat{V}_{\text{s}',l'}^\dagger(t')] = \delta_{\text{s,s}'}\, \delta_{l,l'}\, \delta(t - t')$ and $[\hat{W}_{\text{s}}(t), \hat{W}_{\text{s}'}^\dagger(t')] = \delta_{\text{s,s}'}\, \delta(t - t')$, with the $\hat{V}$ and $\hat{W}$ operators uniformly commuting as well.

3.2. Semiclassical formalism

The quantum formalism is required when certain phenomena such as spontaneous parametric down conversion need to be investigated in depth. In our system, we are only interested in the macroscopic and deterministic behavior of these intracavity fields, and therefore, only the stimulated effects are of interest. In that case, the approach where the fields are treated semiclassically is appropriate and provides sufficient accuracy.

Passing from the quantum to the semiclassical model corresponds to transformations where the creation and annihilation operators are transformed into complex-valued, slowly-varying

Optics EXPRESS

envelopes variables, following $\hat{a}_l \rightarrow \mathcal{A}_l$, $\hat{a}_l^\dagger \rightarrow \mathcal{A}_l^*$, $\hat{c} \rightarrow C$, and $\hat{c}^\dagger \rightarrow C^*$. By analogy to the photon number operators $\hat{a}_l^\dagger \hat{a}_l$ and $\hat{c}^\dagger \hat{c}$, the real-valued quantities $\mathcal{A}_l^* \mathcal{A}_l \equiv |\mathcal{A}_l|^2$ correspond to the number of optical photons in the mode l, while $C^* C \equiv |C|^2$ is the number of microwave photons in the RF strip cavity. Both these photon number quantities are dimensionless, and so are $\mathcal{A}_l$ and C. However, one should note that while $\mathcal{A}_l$ and C are cavity fields, the input fields $\mathcal{A}_{\rm in}$ and $C_{\rm in}$ are propagating fields: They are such that $|\mathcal{A}_{\rm in}|^2$ and $|C_{\rm in}|^2$ correspond to photon fluxes (i. e., number of photons per second) entering the modulator when the optical and microwave input powers are $P_{\rm L}$ and $P_{\rm M}$, respectively. Therefore, the unit of the input fields $\mathcal{A}_{\rm in}$ and $C_{\rm in}$ is $\mathrm{s}^{-1/2}$.

In our analysis, we are only interested in the deterministic dynamics of the intracavity fields, and therefore we can disregard the quantum fluctuations (along with any other stochastic influence). Consequently, the quantum Eqs. (6) and (7) can now be rewritten under the following semiclassical form:

$$\dot{\mathcal{A}}_l = -\kappa(1 + i\alpha)\mathcal{A}_l - ig[C\mathcal{A}_{l-1} + C^*\mathcal{A}_{l+1}] + \delta(l)\sqrt{2\kappa_{\rm e}}\,\mathcal{A}_{\rm in} \tag{8}$$

$$\dot{C} = -\mu(1 + i\xi)C - ig\sum_m \mathcal{A}_m^*\mathcal{A}_{m+1} + \sqrt{2\mu_{\rm e}}\,C_{\rm in}\,, \tag{9}$$

where the new dynamical variables of the system are the complex-valued cavity field envelopes $\mathcal{A}_l$ and C, of respective carrier frequencies $\omega_{\rm L} + l\Omega_{\rm R}$ and $\Omega_{\rm R}$.

3.3. Output microwave and optical fields

The output optical fields are expressed as

$$\mathcal{A}_{{\rm out},l} = -\mathcal{A}_{\rm in}\,\delta(l) + \sqrt{2\kappa_{\rm e}}\,\mathcal{A}_l\,. \tag{10}$$

for each mode l, and the total output field is

$$\mathcal{A}_{\rm out} = \sum_l \mathcal{A}_{{\rm out},l}\,e^{il\Omega_{\rm R}t}\,. \tag{11}$$

Note that $\mathcal{A}_{\rm out}$ is a propagating field like $\mathcal{A}_{\rm in}$ (and not a cavity field like $\mathcal{A}_l$), and consequently, its square modulus $|\mathcal{A}_{\rm out}|^2$ is also a photon flux with units of s^{-1}. The corresponding optical output power in units of watts is

$$P_{\rm opt,\,out} = \hbar\omega_{\rm L}\,|\mathcal{A}_{\rm out}|^2\,, \tag{12}$$

and the optical power transmission coefficient of the modulator is therefore $|\mathcal{T}_{\rm opt}|^2 = P_{\rm out}/P_{\rm in} = \hbar\omega_{\rm L}|\mathcal{A}_{\rm out}|^2/P_{\rm L} \in [0, 1]$. In comparison, the transmission coefficient for a typical Mach-Zehnder electrooptical modulator is defined instead as $|\mathcal{T}_{\rm opt}|^2 = P_{\rm out}/P_{\rm in} = \cos^2[x + \phi] \in [0, 1]$, where x and ϕ are the suitably normalized RF and bias voltages.

As far as the microwave output power is concerned, we note that an infinite-bandwidth photodetector would output a RF signal proportional to the incoming optical power, and we can write

$$V_{\rm PD}(t) = SP_{\rm opt,\,out} = \hbar\omega_{\rm L}\,S|\mathcal{A}_{\rm out}|^2\,, \tag{13}$$

where $V_{\rm PD}(t)$ is in volts, while S is the sensitivity of the photodiode in units of V/W. The generated microwave would be a multi-harmonic signal, and would feature spectral components of frequency $n \times \Omega_{\rm R}$, with $n = 0, 1, 2, \ldots$ The voltage output of the photodiode can therefore be Fourier-expanded as

$$V_{\rm PD}(t) = \frac{1}{2}\mathcal{M}_0 + \sum_{n=1}^{+\infty}\left[\frac{1}{2}\mathcal{M}_n\,\exp(in\Omega_{\rm R}t) + \text{c. c.}\right] \equiv \sum_{n=0}^{+\infty} V_{{\rm PD},n}(t)\,, \tag{14}$$

Optics EXPRESS

where c. c. stands for the complex conjugate of the preceding terms, and

$$\mathcal{M}_n = 2\hbar\omega_{\mathrm{L}}\, S \sum_m \mathcal{A}^*_{\mathrm{out},m}\mathcal{A}_{\mathrm{out},m+n} \tag{15}$$

is the complex slowly-varying envelope corresponding to the microwave spectral component $V_{\mathrm{PD},n}(t)$ of frequency $n \times \Omega_{\mathrm{R}}$ (in volts). The microwave power for the harmonic of frequency $n \times \Omega_{\mathrm{R}}$ can then be evaluated as

$$P_{\mathrm{rf},0} = \frac{|\mathcal{M}_0|^2}{4R_{\mathrm{out}}} \quad \text{and} \quad P_{\mathrm{rf},n} = \frac{|\mathcal{M}_n|^2}{2R_{\mathrm{out}}} \quad \text{for} \quad n \geq 1\,, \tag{16}$$

where R_{out} is the characteristic load resistance in the RF branch.

4. Closed-loop configuration: miniature OEO

4.1. Model

The miniature OEO corresponds to the closed-loop system where the output microwave signal of the photodetector is used to feed the RF electrode of the WGM electrooptical modulator. In order to mathematically describe this physical procedure, we assume that only the fundamental tone $\mathcal{M}_1$ [see Eq. (15)] with frequency Ω_{R} of the photodetected optical signal is fed back to the RF electrode of the modulator, while the DC and higher-harmonic tones are filtered out. Analogously to Eq. (5), we can determine that the microwave photon flux after the photodetector is $P_{\mathrm{rf},1}/\hbar\Omega_{\mathrm{R}}$, where $P_{\mathrm{rf},1}$ is the power of the fundamental tone as defined in Eq. (16). In order to close the oscillation loop, the corresponding voltage signal is subsequently amplified and phase-shifted before being injected in the RF electrode of the electrooptical modulator. The envelope of the normalized microwave signal at the input port of the WGM modulator is now defined as

$$C_{\mathrm{in,OEO}} = \Gamma e^{i\Phi}[2R_{\mathrm{out}}\,\hbar\Omega_{\mathrm{R}}]^{-\frac{1}{2}}\,\mathcal{M}_1\,, \tag{17}$$

where $\Gamma \geq 0$ is the real-valued dimensionless feedback gain, which is controlled by an RF amplifier just after the photodiode. All the loop losses are lumped into the feedback term Γ as well (including the portion of the RF signal that is outcoupled for technological utilization, but excluding the strip and WGM resonator losses). We can therefore express the gain as

$$\Gamma = G_{\mathrm{A}}G_{\mathrm{L}}\,, \tag{18}$$

where G_{A} (≥ 1) is the RF amplifier gain, while G_{L} (≤ 1) is the loss factor of the electric branch. The parameter Φ stands for the microwave rountrip phase shift, that can be adjusted to any value (modulo 2π) using the in-loop RF phase shifter. From the technological perspective, it is useful to note that the output optical signal (electrooptical comb) of the miniature OEO is proportional to $\mathcal{A}_{\mathrm{out}}$, while the microwave output signal is proportional to $\mathcal{M}_1$. In the later case, the RF power at the output of the photodiode is $P_{\mathrm{rf},1}$, while the microwave power of the signal after the amplifier is

$$P_{\mathrm{rf,out}} = \hbar\Omega_{\mathrm{R}}\,|C_{\mathrm{in,OEO}}|^2 = \Gamma^2\frac{|\mathcal{M}_1|^2}{2R_{\mathrm{out}}} = \Gamma^2 P_{\mathrm{rf},1}\,, \tag{19}$$

and it corresponds to the maximal RF power generated in the miniature OEO feedback loop.

Optics EXPRESS

By replacing C_{in} by $C_{\text{in,OEO}}$ in Eq. (9), we obtain the closed-loop model for the miniature OEO as

$$\dot{\mathcal{A}}_l = -\kappa(1+i\alpha)\mathcal{A}_l - ig[C\mathcal{A}_{l-1} + C^*\mathcal{A}_{l+1}] + \delta(l)\sqrt{2\kappa_{\text{e}}}\,A_{\text{in}} \tag{20}$$

$$\begin{aligned}\dot{C} = &-\mu(1+i\xi)C - ig\sum_m \mathcal{A}_m^*\mathcal{A}_{m+1} \\ &+ \Gamma e^{i\Phi}\,\eta\left\{2\kappa_{\text{e}}\sum_m \mathcal{A}_m^*\mathcal{A}_{m+1} - A_{\text{in}}\sqrt{2\kappa_{\text{e}}}(\mathcal{A}_{-1}^* + \mathcal{A}_1)\right\},\end{aligned} \tag{21}$$

where the dimensionless constant

$$\eta = 2\hbar\omega_{\text{L}}\,S\sqrt{\frac{1}{2R_{\text{out}}}\frac{2\mu_{\text{e}}}{\hbar\Omega_{\text{R}}}} \tag{22}$$

is a characteristic optoelectronic parameter of the oscillator ($\simeq 3.5\times10^{-3}$ in our case). Obviously, this efficiency coefficient η is larger when the photodetector sensitivity S is increased; it increases as well when Ω_{R} is decreased, that is, when the resonator is enlarged. This is due to the fact that the electrical energy yields more microwave photons when their individual energy quantum is lower. This phenomenology indicates that high-Q mm-size WGM resonators, which are characterized by GHz-range FSRs, are the most suitable form that perspective.

The reader can note that the overall electrical gain of the feedback loop is in fact the parameter $\beta = \eta\Gamma e^{i\Phi}$, which weights the efficiency of the process that retrieves microwave energy from the output electrooptical comb generated by the WGM modulator via photodetection, and feeds it back as an electrical signal inside the RF strip cavity of the modulator. Also note that since our input optical field $\mathcal{A}_{\text{in}}$ is real-valued [see Eq. (5)], we can drop the calligraphic notation and simply write it as A_{in}: it means that we have arbitrarily set its phase to 0, and as a consequence, the optical phase to all the intracavity fields $\mathcal{A}_l$ is determined with regard to the pump laser field.

4.2. Numerical simulation of the temporal dynamics

Equations (20) and (21) govern the dynamics of the miniature OEO, and permit to undertake a complete theoretical analysis of that closed-loop system. In particular, they allow us to achieve a deep understanding of the system's temporal dynamics via numerical simulation as the gain Γ is varied. Figure 3 displays numerical simulations performed with the fourth-order Runge-Kutta algorithm, and we have considered a total of 41 modes ($l = -20, \ldots, 20$). The initial conditions are set such that there are a few photons in the optical modes and in the RF cavity ($|\mathcal{A}_l(0)|^2 \sim |C(0)|^2 \sim 1$), and the field variables have random phases. The laser detuning is set at $\alpha = 0.5$, and the loop phase shift is $\Phi = 0$. The top row displays the time-domain dynamics of some output optical modes $P_{\text{opt,out},l} = \hbar\omega_{\text{L}}\,|\mathcal{A}_{\text{out},l}|^2$, where $\mathcal{A}_{\text{out},l}$ is defined in Eq. (10). We have numerically observed, as expected, that the dynamics of a given mode l is of the same order of magnitude (but not identical) to the one of its mirror mode $-l$: for that reason, we have only plotted the modes $l \geq 0$ in order to avoid crowding the figures with redundant plots. The bottom row displays the temporal dynamics of the RF signal at the output of the amplifier, i. e. $P_{\text{rf,out}}$ as defined in Eq. (19).

For the chosen parameters, numerical simulations asymptotically yield a non-null value for the pumped mode $l = 0$, but a null amplitude for the sidemodes $l \neq 0$ when Γ<10.97, leading to a null RF output as well. Once the feedback gain Γ is set to a value higher than 10.97, the sidemodes dynamics eventually leads to constant non-zero amplitudes, and an RF signal is generated. We have not observed here metastable (unusually long) transient behavior as it can sometimes be the case in conventional OEOs (see Ref. [40]).

When $\Gamma = 12$, Fig. 3(a) shows that the pumped mode becomes depleted and exchanges energy with the modes $l = \pm1$, which subsequently settle to a non-null constant value. The dynamics of

Optics EXPRESS

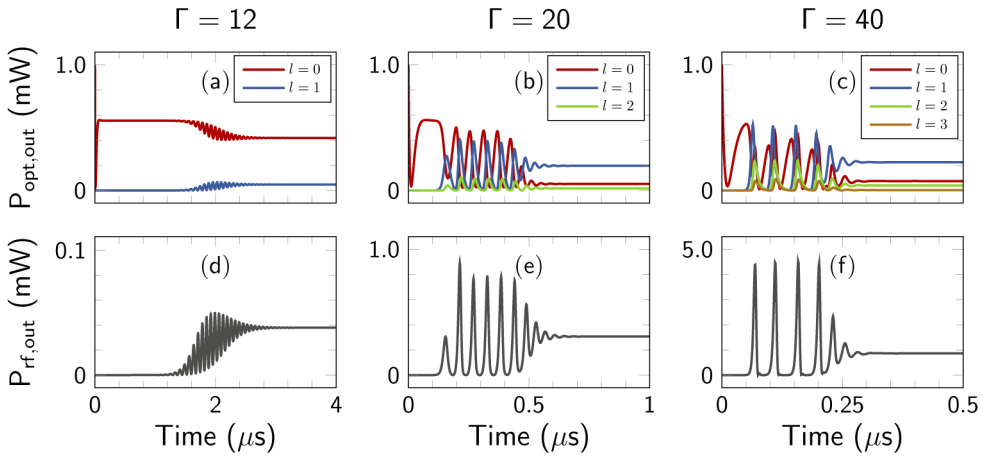

Fig. 3. Time domain dynamics for the optical and microwave power, obtained via the numerical simulation the model presented in Eqs. (20) and Eqs. (21) for $\alpha = 0.5$ and $\Phi = 0$. The different columns correspond to different values of the feedback gain. The top row displays the temporal dynamics of some output optical modes $P_{\mathrm{opt,out},l} = \hbar\omega_{\mathrm{L}}\,|\mathcal{A}_{\mathrm{out},l}|^2$, while the bottom row displays the temporal dynamics of the microwave signal $P_{\mathrm{rf,out}} = \Gamma^2|\mathcal{M}_1|^2/2R_{\mathrm{out}}$ at the output of the RF amplifier. The critical value of the gain below which there is asymptotically no sidemode and RF oscillation is $\Gamma_{\mathrm{cr}} \simeq 10.97$.

the other sidemodes ($|l| \geq 2$) is still negligible at this point. As shown in Fig. 3(d), this process generates a RF signal at the same timescale, with $P_{\mathrm{rf,out}} \simeq 0.04$ mW. When the gain is increased to $\Gamma = 20$ [Fig. 3(b)], the energy exchange from the pump to the sidemodes is more pronounced, and eventually leads to the situation where the output power in the sidemodes $l = \pm 1$ is higher than the one in the pumped mode $l = 0$ (note however that these are *output* fields, and *not* intracavity fields). The sidemode pair $l = \pm 2$ starts to have a noticeable amplitude as well. The RF signal dynamics displays a transient behavior qualitatively similar to the one of the optical modes, before settling to a steady-state value $P_{\mathrm{rf,out}} \simeq 0.3$ mW [Fig. 3(e)]. As shown in Fig. 3(c), further increase of the gain to $\Gamma = 40$ leads to higher complexity in the pump-to-sidemode power conversion, so that the sidemode pair $l = \pm 3$ starts to display sizable oscillations as well. Accordingly, the RF signal settles to a higher value with $P_{\mathrm{rf,out}} \simeq 0.9$ mW [Fig. 3(f)].

Several trends can be outlined in the OEO dynamics as the feedback gain Γ is increased. We can first observe that the output optical modes always have a power that is of the order of the laser pump (here, $P_{\mathrm{L}} = 1$ mW), and that the benefit of increasing the feedback gain is to improve the conversion efficiency from the pump to the sidemodes (up to a certain extent). The top row consistently shows the excitation of additional pairs of sidemodes as the gain is increased, thereby confirming that the WGM resonator plays the role of a dynamical frequency converter. The second observation is that while the optical power is only redistributed amongst the side modes, the RF power steadily increases with the gain. The third observation is that when the gain becomes larger, the transient dynamics is shortened while remaining in the μs timescale (set by the κ photon loss rates). However, this shortened transient dynamics induces pronounced, sharply peaked relaxation oscillations. In the next sub-section, we will investigate the stability properties of our time-domain model and define the conditions under which self-starting oscillations are triggered in the miniature OEO.

Optics EXPRESS

4.3. Stability analysis and threshold gain

When the gain parameter Γ is null, the system receives no RF excitation and the steady state solution of Eqs. (20) and (21) can be straightforwardly derived as

$$C = 0 \quad \text{and} \quad \mathcal{A}_l = \begin{cases} \frac{\sqrt{2\kappa_e}}{\kappa(1+i\alpha)} A_{\text{in}} & \text{if } l = 0 \\ 0 & \text{if } l \neq 0 \end{cases} . \tag{23}$$

This solution is the trivial equilibrium of our oscillator, and it corresponds to a situation where none of the sidemodes with $l \neq 0$ is excited. When Γ is very low, conventional wisdom from self-oscillators theory (confirmed by our numerical simulations in the previous subsection) suggest that the same situation should prevail, i.e, the trivial solution represented in Eq. (28) should remain stable. However, as the gain is increased, there should be a critical value Γ_{cr} beyond which self-sustained oscillations are obtained, with asymptotic values $C \neq 0$ and $\mathcal{A}_l \neq 0$. The objective of this subsection if to find Γ_{cr} analytically.

In order to determine the linear stability of the trivial fixed point of Eq. (23), we need to find the Jacobian of the flow corresponding to Eqs. (20) and (21). If we consider an electrooptical comb with $2N + 1$ sidemodes, the variables of the perturbation flow are $\delta\mathcal{A}_l$ with $l = -N, \ldots, N$ and δC, i.e., the dimensionality of this flow is $2N + 2$ and the Jacobian around the trivial solution is an $(2N + 2) \times (2N + 2)$ complex-valued matrix. However, one can note that the perturbations $\delta\mathcal{A}_l$ with $|l| \geq 2$ are of second order and do not influence the eigenvalue spectrum of this Jacobian. This is due to the fact that the first sidemodes to be excited in electrooptical combs are necessarily the ones adjacent to the pumped mode, with $l = \pm 1$, and from there the comb sequentially grows "outwards" in the frequency domain. In other words, the sidemodes $l = \pm 2, \pm 3, \pm 4, \ldots$ are excited through a cascaded mechanism that require the modes $l = \pm 1, \pm 2, \pm 3, \ldots$ to be excited beforehand. This phenomenology is similar to the one observed in WGM OEOs with Mach-Zehnder modulators (see Ref. [15]), but quite different from the one observed in Kerr comb formation where the first modes to be excited via modulational instability are not necessarily adjacent to the pumped mode [10,41].

Along with the perturbations $\delta\mathcal{A}_l$ with $|l| \geq 2$, the perturbation $\delta\mathcal{A}_0$ of the pumped mode is also irrelevant for the stability analysis, because it is a neutrally stable with a null eigenvalue. Therefore, stability analysis is drastically reduced from $2N + 2$ to 3 perturbation variables, namely $\delta\mathcal{A}_{-1}$, $\delta\mathcal{A}_1$ and δC, which obey the linearized autonomous flow

$$\begin{aligned} \delta\dot{\mathcal{A}}^*_{-1} &= -\kappa\,(1 - i\alpha)\,\delta\mathcal{A}^*_{-1} + ig\mathcal{A}^*_0\delta C \\ \delta\dot{\mathcal{A}}_1 &= -\kappa\,(1 + i\alpha)\,\delta\mathcal{A}_1 - ig\mathcal{A}_0\delta C \\ \delta\dot{C} &= -\mu\,(1 + i\xi)\,\delta C + \left[(2\kappa_e\beta - ig)\mathcal{A}_0 - \beta\sqrt{2\kappa_e}A_{\text{in}}\right]\delta\mathcal{A}^*_{-1} \\ &\quad + \left[(2\kappa_e\beta - ig)\mathcal{A}^*_0 - \beta\sqrt{2\kappa_e}A_{\text{in}}\right]\delta\mathcal{A}_1\,, \end{aligned} \tag{24}$$

where $\mathcal{A}_0$ is explicitly defined via Eq. (28), while $\beta = \eta\Gamma e^{i\Phi}$ is the overall gain parameter in the electrical branch. The Barkhausen phase condition for autonomous oscillators imposes that β should be real-valued, i.e. the phase shifter should be set such that $\Phi = 0$ or π (modulo 2π) – as we will see later on, the appropriate sign for β will actually depend on the sign of α.

The complex-valued flow in Eq. (24) can be rewritten under the matrix form as $\delta\dot{\mathbf{X}} = \mathbf{J} \cdot \delta\mathbf{X}$, where $\delta\mathbf{X} = [\delta\mathcal{A}^*_{-1}, \delta\mathcal{A}_1, \delta C]^{\text{T}}$ is the perturbation vector and $\mathbf{J}$ is the 3×3 Jacobian whose eigenvalues will decide the stability of the trivial fixed point. From the analytical point of view, it is mathematically difficult investigate the spectral stability of a three-dimensional Jacobian when it is complex-valued. However, this task is mathematically more tractable for real-valued Jacobian matrices. For this reason, we transform the complex-valued flow of Eq. (24) into a

Optics EXPRESS

real-valued one by decomposing the perturbation vector and the Jacobian into their real and imaginary parts, following $\delta\mathbf{X} = \delta\mathbf{X}_\mathrm{r} + i\mathbf{X}_\mathrm{i}$, and $\delta\mathbf{J} = \delta\mathbf{J}_\mathrm{r} + i\mathbf{J}_\mathrm{i}$. As a consequence, by plugging these decompositions into the autonomous flow $\delta\dot{\mathbf{X}} = \mathbf{J}\cdot\delta\mathbf{X}$, we find that Eq. (24) can now be rewritten under the form of a six-dimensional real-valued flow following

$$\begin{bmatrix} \delta\dot{\mathbf{X}}_\mathrm{r} \\ \delta\dot{\mathbf{X}}_\mathrm{i} \end{bmatrix} = \mathbf{J}_\mathrm{ri}\begin{bmatrix} \delta\mathbf{X}_\mathrm{r} \\ \delta\mathbf{X}_\mathrm{i} \end{bmatrix} \quad \text{with} \quad \mathbf{J}_\mathrm{ri} = \begin{bmatrix} \mathbf{J}_\mathrm{r} & -\mathbf{J}_\mathrm{i} \\ \mathbf{J}_\mathrm{i} & \mathbf{J}_\mathrm{r} \end{bmatrix} \tag{25}$$

being the expanded Jacobian, while the sub-matrices $\mathbf{J}_\mathrm{r}$ and $\mathbf{J}_\mathrm{i}$ are explicitly defined as

$$\mathbf{J}_\mathrm{r} = \begin{bmatrix} -\kappa & 0 & p_g \\ 0 & -\kappa & p_g \\ (p_\beta + p_g) & (p_\beta - p_g) & -\mu \end{bmatrix} \text{ and } \mathbf{J}_\mathrm{i} = \begin{bmatrix} \kappa\alpha & 0 & q_g \\ 0 & -\kappa\alpha & -q_g \\ -(q_g - q_\beta) & -(q_g + q_\beta) & -\mu\xi \end{bmatrix}, \tag{26}$$

with $q_g = g\mathrm{Re}(\mathcal{A}_0)$, $p_g = g\mathrm{Im}(\mathcal{A}_0)$, $p_\beta = \beta[2\kappa_\mathrm{e}\mathrm{Re}(\mathcal{A}_0) - \sqrt{2\kappa_\mathrm{e}}A_\mathrm{in}]$, and $q_\beta = 2\kappa_\mathrm{e}\beta\mathrm{Im}(\mathcal{A}_0)$. Without loss of generality, we will simplify the calculations in the remainder of the article by considering that the microwave signal fed back to the RF strip resonator is resonant, i.e. $\xi = 0$.

The trivial fixed point of Eq. (28) is linearly stable (i.e., the OEO does *not* oscillate) when the real parts of all the eigenvalues of the Jacobian matrix $\mathbf{J}_\mathrm{ri}$ are strictly negative. These eigenvalues are solution of the 6-th order characteristic polynomial

$$\det[\mathbf{J}_\mathrm{ri} - \lambda\mathbf{I}_6] = \sum_{k=0}^{6} m_{6-k}\lambda^k = 0\,, \tag{27}$$

where the real-valued polynomial coefficients are explicitly defined as

$$m_0 = 1 \tag{28}$$

$$m_1 = 2\,(2\kappa + \mu) \tag{29}$$

$$m_2 = -4p_g p_\beta + 4q_g q_\beta + 2\left(3 + \alpha^2\right)\kappa^2 + 8\kappa\mu + \mu^2 \tag{30}$$

$$\begin{aligned} m_3 = 4\Big\{ & q_g\left[q_\beta\,(3\kappa + \mu) + p_\beta\alpha\kappa\right] + \kappa\left[\left(1 + \alpha^2\right)\kappa^2 + \left(3 + \alpha^2\right)\kappa\mu + \mu^2\right] \\ & + p_g\left[q_\beta\alpha\kappa - p_\beta\,(3\kappa + \mu)\right]\Big\} \end{aligned} \tag{31}$$

$$\begin{aligned} m_4 = {} & 4\left(q_g^2 q_\beta^2 + p_g^2 p_\beta^2\right) + \kappa\left[\left(1 + \alpha^2\right)^2\kappa^2 + 8\left(1 + \alpha^2\right)\kappa\mu + 2\left(3 + \alpha^2\right)\mu^2\right] \\ & + 4\kappa\left[\left(q_g q_\beta - p_g q_\beta\right)\left(3\kappa + \alpha^2\kappa + 3\mu\right) + \alpha\left(q_g q_\beta + p_g q_\beta\right)(2\kappa + \mu)\right] \\ & - 8q_g p_g p_\beta q_\beta \end{aligned} \tag{32}$$

$$\begin{aligned} m_5 = {} & 2\kappa\left[2q_g\left(p_\beta\alpha + q_\beta\right) - 2p_g\left(p_\beta - q_\beta\alpha\right) + \left(1 + \alpha^2\right)\kappa\mu\right] \\ & \times\left[-2p_g p_\beta + 2q_g q_\beta + \kappa\left(\kappa + \alpha^2\kappa + 2\mu\right)\right] \end{aligned} \tag{33}$$

$$\begin{aligned} m_6 = \kappa^2\Big\{ & 4\alpha^2\left(q_g^4 + p_g^4\right) + 4q_g^2\left(q_\beta + p_\beta\alpha\right)^2 + 4p_g^2\left[p_\beta^2 - 2p_\beta q_\beta\alpha + \left(2q_g^2 + q_\beta^2\right)\alpha^2\right] \\ & + 4q_g\left(q_\beta + p_\beta\alpha\right)\left(1 + \alpha^2\right)\kappa\mu + \left(1 + \alpha^2\right)^2\kappa^2\mu^2 \\ & - 4p_g\left(p_\beta - q_\beta\alpha\right)\left[2q_g\left(q_\beta + p_\beta\alpha\right) + \left(1 + \alpha^2\right)\kappa\mu\right]\Big\}. \end{aligned} \tag{34}$$

Optics EXPRESS

The Routh-Hurwitz theorem states a necessary and sufficient condition for all the eigenvalues of the characteristic polynomial of Eq. (27) to have strictly negative real parts is to fulfill the inequalities

$$\Delta_i = \begin{vmatrix} m_1 & m_0 & 0 & 0 & 0 & \cdots & 0 & 0 \\ m_3 & m_2 & m_1 & m_0 & 0 & \cdots & \cdots & \cdots \\ m_5 & m_4 & m_3 & m_2 & m_1 & \cdots & \cdots & \cdots \\ m_7 & m_6 & m_5 & m_4 & m_3 & \cdots & \cdots & \cdots \\ \cdots & \cdots & \cdots & \cdots & \cdots & \cdots & \cdots & \cdots \\ \cdots & \cdots & \cdots & \cdots & \cdots & \cdots & \cdots & \cdots \\ \cdots & \cdots & \cdots & \cdots & \cdots & \cdots & m_{i-1} & m_{i-2} \\ \cdots & \cdots & \cdots & \cdots & \cdots & \cdots & m_{i+1} & m_i \end{vmatrix} > 0 \quad \text{for} \quad i = 1, \ldots, 6 . \tag{35}$$

The numerical computation of the determinants Δ_i as Γ is varied shows that the lowest-order critical determinant that fails to fulfill this inequality is Δ_3. The direct numerical computation of the eigenvalue spectrum for both $\mathbf{J}$ and $\mathbf{J}_{\mathrm{ri}}$ confirms that at least one eigenvalue transversely crosses the imaginary axis when $\Delta_3 = 0$. The critical gain value Γ_{cr} needed to trigger the oscillations is therefore a root of the algebraic equation

$$\Delta_3 = m_1 m_2 m_3 - m_1^2 m_4 - m_0 m_3^2 + m_0 m_1 m_5 = a[\Gamma e^{i\Phi}]^2 + b[\Gamma e^{i\Phi}] + c = 0 \tag{36}$$

with

$$a = 128\eta^2\alpha^2\kappa_{\mathrm{e}}^2 g^2 A_{\mathrm{in}}^4 \frac{(\kappa - \kappa_{\mathrm{e}})(\mu + 2\kappa_{\mathrm{e}})}{\kappa^2 \left(1 + \alpha^2\right)^2} \tag{37}$$

$$\begin{aligned} b = -16\eta\alpha g A_{\mathrm{in}}^2 \frac{\kappa_{\mathrm{e}}}{\kappa\left(1+\alpha^2\right)} \Big\{ & 4\left(1+\alpha^2\right)\kappa^4 + \mu^3(\mu + 2\kappa_{\mathrm{e}}) + 2\kappa\mu^2(3\mu + 4\kappa_{\mathrm{e}}) \\ & + 2\kappa^3\left[8\mu - 2\kappa_{\mathrm{e}}\left(-3+\alpha^2\right)\right] + \kappa^2\mu\left[\left(17+\alpha^2\right)\mu + 2\kappa_{\mathrm{e}}\left(9+\alpha^2\right)\right] \Big\} \end{aligned} \tag{38}$$

$$\begin{aligned} c = 8\kappa \Big[& 8\left(1+\alpha^2\right)\kappa^5 + \left(29 + 14\alpha^2 + \alpha^4\right)\kappa^4\mu + 8\left(5+\alpha^2\right)\kappa^3\mu^2 \\ & + 2\left(13+\alpha^2\right)\kappa^2\mu^3 + 8\kappa\mu^4 + \mu^5 \Big] . \end{aligned} \tag{39}$$

The solution to the quadratic Eq. (36) is

$$\Gamma_{\mathrm{cr}\pm} e^{i\Phi} = -\frac{K_1}{A_{\mathrm{in}}^2}\left[\frac{1}{\alpha}K_2 \pm \frac{1}{|\alpha|}K_3\right] \tag{40}$$

where

$$K_1 = \frac{-\left(1+\alpha^2\right)\kappa}{16\eta g\kappa_{\mathrm{e}}(\kappa - \kappa_{\mathrm{e}})(\mu + 2\kappa_{\mathrm{e}})} \tag{41}$$

$$\begin{aligned} K_2 = {} & 4\kappa^4\left(1+\alpha^2\right) + \mu^3(\mu + 2\kappa_{\mathrm{e}}) + 2\kappa\mu^2(3\mu + 4\kappa_{\mathrm{e}}) + 2\kappa^3\left[8\mu - 2\kappa_{\mathrm{e}}(\alpha^2 - 3)\right] \\ & + \kappa^2\mu\left[\mu\left(17+\alpha^2\right) + 2\kappa_{\mathrm{e}}\left(9+\alpha^2\right)\right] \end{aligned} \tag{42}$$

$$\begin{aligned} K_3 = (2\kappa + \mu) \Big\{ & -2\kappa^3\left(1+\alpha^2\right) + \mu^2(\mu + 2\kappa_{\mathrm{e}}) + 2\kappa\mu(2\mu + 6\kappa_{\mathrm{e}}) \\ & + \kappa^2\left[\mu\left(1+\alpha^2\right) + 2\kappa_{\mathrm{e}}\left(5+\alpha^2\right)\right] \Big\} \end{aligned} \tag{43}$$

Optics EXPRESS

Equation (40) involves two branches of solutions, the first one being $-K_1\,(K_2-K_3)\,/(\alpha A_{\rm in}^2)$ and the second one being $-K_1\,(K_2+K_3)\,/(\alpha A_{\rm in}^2)$. However, the second branch yields solutions that are about two orders of magnitude larger than the first one in absolute value: these solutions are unphysical and can be discarded in our current configuration.

Therefore, we finally obtain the following formula for the critical feedback gain

$$\Gamma_{\rm cr} = -\frac{K_1}{A_{\rm in}^2\,\alpha e^{i\Phi}}\,(K_2-K_3) > 0 \quad \text{with} \quad \begin{cases} \Phi = 0 & \text{if } \alpha > 0 \\ \Phi = \pi & \text{if } \alpha < 0 \end{cases} . \tag{44}$$

The miniature OEO is expected to oscillate when the feedback gain is such that $\Gamma > \Gamma_{\rm cr}$, and we observe that the feedback phase Φ has to be adjusted differently depending on the sign of α, i.e., depending on the direction of the detuning from resonance in the pumped mode.

Figure 4 displays the variations of $\Gamma_{\rm cr}$ as a function of the optical detuning α. One can obseerve that the curve is symmetric with regard to axis of symmetry at $\alpha = 0$. Moreover, $\Gamma_{\rm cr}$ diverges when $\alpha \longrightarrow 0$ and when $\alpha \longrightarrow \pm\infty$. This can be understood in first aproximation via the variations of the output field $\mathcal{A}_{\rm out,0} = A_{\rm in}\,[2\kappa_{\rm e}/\kappa\,(1+i\alpha) - 1]$. On the one hand, when $\alpha \longrightarrow 0$, the pump is resonant and accordingly $\mathcal{A}_{\rm out,0}$ is weak, so that the comb photodetection voltage is low – thus requiring a high gain Γ to offset this power deficit. On the other hand, when $\alpha \longrightarrow \pm\infty$, the coupling is weak and so is $\mathcal{A}_0$, so that the electrooptical comb generation is poor and the photodetection signal is low as well. Therefore, it appears that optimal operation of the miniature OEO (i.e., low threshold feedback gain $\Gamma_{\rm cr}$) requires to detune the pump laser in between these two asymptotic cases.

Figure 5 shows the bifurcation diagrams for the optical output signals $P_{{\rm opt,out},l}$, for the microwave power $P_{\rm rf,1}$, and for the RF power $P_{\rm rf,out}$ generated at the output of the RF amplifier as the gain Γ is varied. The first salient feature is that the optical power in paired modes $\pm l \neq 0$ displays a switching behavior, with $P_{{\rm opt,out},l} \neq P_{{\rm opt,out},-l}$: However, the power in the pumped mode $l = 0$ and in the RF signals varies smoothly with the gain. This behavior is quite different from the one observed in Kerr optical frequency combs, for example, where paired modes typically have the same power [8–10]. The second observation that can be made is that quantitatively, $P_{\rm rf,1} \ll P_{\rm rf,out}$, with a ratio that can grow up to four orders of magnitude in our simulations. The third note is

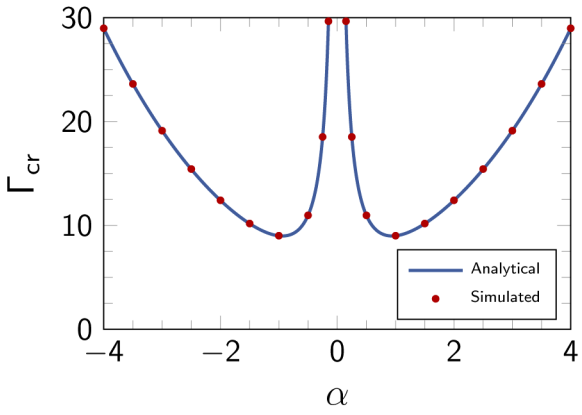

Fig. 4. Variation of the critical feedback strength $\Gamma_{\rm cr}$ as a function of α. The symbols are obtained via the numerical simulation of the time-domain OEO model presented in Eqs. (20) and (21), while the solid line corresponds to the analytical solution provided in Eq. (44). It can be seen that the stability analysis permits to determine the threshold gain needed to trigger microwave oscillations with exactitude. It also appears that minimum gain is achieve for $\alpha \simeq \pm 1$.

Optics EXPRESS

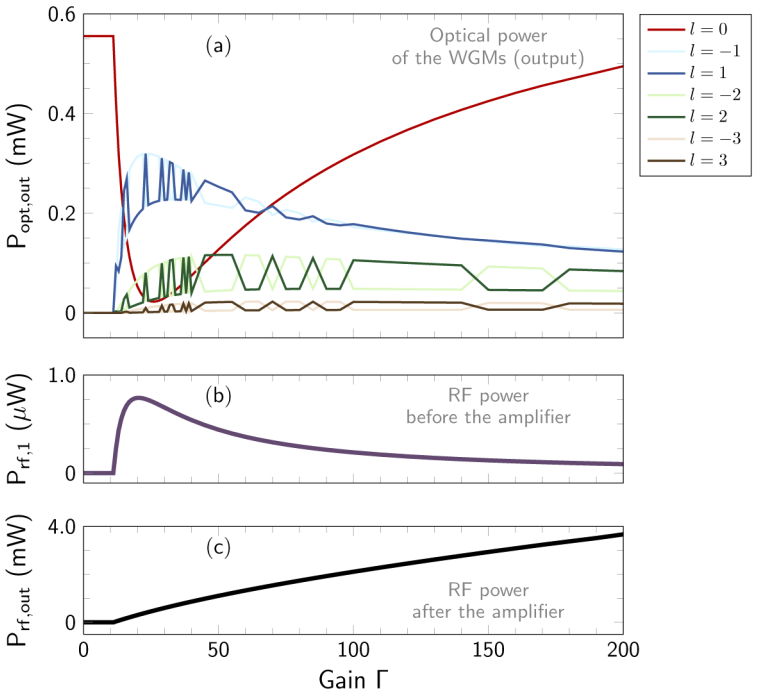

Fig. 5. Bifurcation diagrams for the optical output signals $P_{\mathrm{opt,out},l}$, for the microwave power $P_{\mathrm{rf},1}$ generated by the photodiode (before the RF amplifier), and for the RF power $P_{\mathrm{rf,out}}$ generated at the output of the RF amplifier. The parameters of the system are the same as those of Fig. 3, with $\alpha = 0.5$ and $\Phi = 0$. The critical value of the gain below which there is no OEO oscillation is $\Gamma_{\mathrm{cr}} \simeq 10.97$, in agreement with Fig. 4. Note that as the gain Γ is increased, there are optical mode power switches within a given sidemode pair $\pm l \neq 0$, while the pumped optical mode $l = 0$ and the RF signals are varying smoothly.

that qualitatively, the RF power $P_{\mathrm{rf},1}$ at the output of the photodiode does not increase steadily, while the power $P_{\mathrm{rf,out}}$ after the amplifier always does.

5. Optimization: system parameters leading to the smallest threshold gain

In this section, we determine the optimal conditions leading to the smallest value of the critical gain Γ_{cr} for the feedback gain.

5.1. Optimal laser detuning from resonance

We first need to find the optimal detuning α_{opt} for which the gain becomes minimal. We look for the roots of the algebraic equation $d(\Gamma_{\mathrm{cr}})/d\alpha = 0$ for $\alpha > 0$, and we are led to the equation:

$$\left(-1 + 2\alpha^2 + 3\alpha^4\right)\kappa^4 + 2\left(-1 + \alpha^2\right)\kappa\mu + \left(-1 + \alpha^2\right)\mu^2 = 0\,, \tag{45}$$

which is bi-quadratic in α. There are two roots $\alpha^2_{\mathrm{opt},\pm}$; The solution $\alpha^2_{\mathrm{opt},-}$ has to be discarded for being negative (and thus, unphysical), while the other solution yields the desired results as

$$\alpha_{\mathrm{opt},+} \equiv \alpha_{\mathrm{opt}} = \pm\frac{1}{\sqrt{6}\kappa}\sqrt{-\left[\kappa^2 + (\kappa+\mu)^2\right] + \sqrt{\left[\kappa^2 + (\kappa+\mu)^2\right]^2 + 12\kappa^2(\kappa+\mu)^2}} \tag{46}$$

The formula above can be simplified: indeed, the miniature OEO is generally configured in a way that the loaded optical resonance linewidth 2κ is much smaller than the loaded RF resonance

Optics EXPRESS

linewidth. If we write this condition as $|\kappa/\mu| \ll 1$ and use this ratio as a smallness parameter, a Taylor expansion of Eq. (46) yields the following expression for the optimal detuning:

$$\alpha_{\text{opt}} \simeq \pm\left[1 - \frac{1}{2}\left(\frac{\kappa}{\mu}\right)^2\right] \simeq \pm 1 \quad \text{when} \quad \frac{\kappa}{\mu} \to 0\,. \tag{47}$$

It therefore appears that the laser driving miniature OEO should ideally be detuned to the edge of the optical resonance, since $\alpha = \pm 1$ translates to $\sigma_{\text{A}} = \pm\kappa$. This is confirmed in Fig. 4 where it can be seen that the critical gain Γ_{cr} is minimal ($\simeq 9$) around $\alpha = \pm 1$. We note that here, despite the fact that we have a relatively high ratio κ/μ ($\simeq 0.23$), the approximation $\alpha_{\text{opt}} = \pm 1$ already appears to be very good, since the exact value given by Eq. (46) is 0.94. As noted above, the precision of this approximation $\alpha_{\text{opt}} = \pm 1$ is expected to increase as $\kappa/\mu \to 0$, i. e., for when the optical resonance becomes increasingly narrower than the microwave one. From a technological perspective, it is interesting to note that this requirement is fortunately not stringent, as the minimum appears to be relatively flat: in other words, a deviation of ±5% with regard to α_{opt} still yields a close-to-minimum critical gain value.

5.2. Optimal resonator coupling coefficient

The objective here is to find the optimal value $\kappa_{\text{e,opt}}$ for the resonator coupling coefficient. One should keep in mind that the intrinsic coupling coefficient κ_{i} is an intrinsic property of the resonator and cannot be tuned. However, κ_{e} can be viewed as a coupling efficiency parameter that is indeed tunable, for example by varying the distance (a few λ_{L}) between the prism and the resonator in Fig. 1. It results that the loaded linewidth 2κ can be varied by the same token.

The critical gain defined in Eq. (44) is written as a function of κ and κ_{e}, which in inconvenient in the present case because both parameters are coupling dependent. We therefore need to rewrite that equation in a way that a single parameter becomes responsible for the variations in coupling strength. For that purpose, it is convenient to introduce the parameter

$$\rho = \frac{\kappa_{\text{e}}}{\kappa} \in [0, 1], \tag{48}$$

which is the ratio between outcoupling and total losses in the resonator. The resonator is in the regime of undercoupling when $0<\rho<\frac{1}{2}$ (most losses are intrinsic), overcoupling when $\frac{1}{2}<\rho<1$ (most losses are extrinsic), and critical coupling when $\rho = \frac{1}{2}$. The limit case $\rho = 0$ corresponds to the situation where the resonator is uncoupled (all losses are intrinsic), while the limit case $\rho = 1$ corresponds to the situation where the intrinsic losses are null (the intrinsic Q-factor is infinite and all losses are coupling-induced). The critical gain defined in Eq. (44) can now be rewritten as a function of the intrinsic loss parameter κ_{i}, and the coupling ratio ρ whose variations from 0 to 1 scan all the possible coupling configurations. It is noteworthy that this coefficient ρ plays a major role in the quantum applications of WGM resonators [42].

In order to find the exact value of the optimal ρ_{opt} (or equivalently, the optimal $\kappa_{\text{e,opt}}$), one has to insert Eq. (46) into Eq. (44), and obtain this optimal value is as the solution of the algebraic equation $d\Gamma_{\text{cr}}/d\rho = 0$. However, this procedure would be cumbersome because the equations involved are algebraically long and complicated. Nevertheless, these calculations can be significantly simplified if we straightforwardly consider the approximation $|\kappa/\mu| \ll 1$ (along with $\alpha_{\text{opt}} \simeq \pm 1$), which give accurate results as shown in Sec. 5.1 dealing with the optimal laser detuning. In that case, the formula for the critical gain can be approximated as

$$\Gamma_{\text{cr}} \simeq \frac{\mu\kappa_{\text{i}}}{g\eta A_{\text{in}}^2 \rho(1-\rho)} \quad \text{when} \quad \frac{\kappa}{\mu} \to 0\,. \tag{49}$$

The formula above yields $\Gamma_{\text{cr}} \simeq 8$ with our parameters, a value that approximates quite well the minimum that is obtained in Fig. 4. Equation (49) also clearly indicates that the critical gain

Optics EXPRESS

needed to trigger the microwave oscillations in the miniature OEO increases when the resonator becomes too undercoupled ($\rho \to 0$) or too overcoupled ($\rho \to 1$). The optimal value ρ_{opt} leading to a minimum critical gain is readily found by solving the algebraic equation $d\Gamma_{\mathrm{cr}}/d\rho = 0$, which therefore leads to the approximation:

$$\rho_{\mathrm{opt}} \simeq \frac{1}{2}, \tag{50}$$

corresponding to critical coupling ($\kappa_{\mathrm{i}} \simeq \kappa_{\mathrm{e}}$ and $Q_{\mathrm{i}} \simeq Q_{\mathrm{e}}$). Numerical simulations indicate that the critical coupling condition is not stringent, and a deviation of ±5% with regard to ρ_{opt} still yields a close-to-minimum critical gain value. This optimal value permits to find the absolute minimum for the critical gain as

$$\Gamma_{\mathrm{min}} \simeq \frac{4\mu\kappa_{\mathrm{i}}}{g\eta A_{\mathrm{in}}^2} = \frac{\omega_{\mathrm{L}}\Omega_{\mathrm{R}}}{gSP_{\mathrm{L}}Q_{\mathrm{i}}}\sqrt{\frac{\hbar R_{\mathrm{out}}}{Q_{\mathrm{M}}}} \propto \frac{1}{gSP_{\mathrm{L}}Q_{\mathrm{i}}\sqrt{Q_{\mathrm{M}}}}. \tag{51}$$

For our parameters, we obtain $\Gamma_{\mathrm{min}} \simeq 4.4$, which is then the absolute minimum gain needed to trigger oscillations in our miniature OEO. The formula from Eq. (51) indicates that the threshold gain can be lowered by increasing the nonlinearity, photodetector sensitivity, and optical power, which was expected; but more importantly, it indicates that increasing the intrinsic Q-factor of the WGM resonator is more effective than increasing the Q-factor of the microwave strip cavity.

6. Threshold laser power in the amplifierless miniature OEO

In the preceding sections, we have analyzed an architecture of miniature OEO where an amplifier is inserted in the electrical branch, and the role of the stability analysis was to find the feedback strength Γ_{cr} needed to self-start the microwave oscillation. We had implicitly assumed that the amplifier had a tunable gain, while the optical power was fixed.

However, it is possible to have instead an amplifier with fixed gain, while the pump laser is power-tunable. The question in this case is to find the critical laser power $P_{\mathrm{L,cr}}$ that is needed to trigger RF oscillations. We can use the results from Sec. 4.3 to solve this problem. Hence, considering the relationships $A_{\mathrm{in}}^2 = P_{\mathrm{L}}/\hbar\omega_{\mathrm{L}}$ and $\Gamma = G_{\mathrm{A}}G_{\mathrm{L}}$, we can use Eq. (44) to derive the critical laser power as

$$P_{\mathrm{L,cr}} = \frac{\Upsilon(\alpha,\rho)}{G_{\mathrm{A}}G_{\mathrm{L}}} \quad \text{with} \quad \Upsilon(\alpha,\rho) \equiv -\hbar\omega_{\mathrm{L}}\frac{K_1}{\alpha e^{i\Phi}}(K_2 - K_3) > 0 \tag{52}$$

where K_1, K_2, K_3, and Φ are the same as in Eq. (44).

It results that high gain amplification allows for lower laser powers, and vice versa. For example, Ilchenko *et al.* have reported in Ref. [43] a miniature OEO where the laser power was around 70 μW while the amplifier had a gain of 45 dB (i. e., $G_{\mathrm{A}} \sim 180$). However, on the other hand, higher laser power permits to use amplifiers with lower gain: In fact, if the optical power is high enough, it is even possible to get rid of the amplifier, thereby leading to an *amplifierless* miniature OEO. The reader can note that amplifierless OEOs have already been demonstrated with conventional fiber-based architectures (see for example Ref. [44]). In our system, eliminating the amplifier mathematically corresponds to set $G_{\mathrm{A}} = 1$ in Eq. (52). As a consequence, the OEO architecture of the miniature OEO presented in Fig. 1 is significantly simplified. The critical laser power needed to trigger RF oscillations in the amplifierless miniature OEO can be exactly calculated as $P_{\mathrm{L,cr}} = \Upsilon(\alpha,\rho)/G_{\mathrm{L}}$.

From this analysis, we can now define the absolute minimal optical power that is needed to trigger microwave oscillations in an amplifierless OEO. The procedure for doing so is to consider negligible electrical losses ($G_{\mathrm{L,opt}} = 1$), optimal laser detuning ($\alpha = \alpha_{\mathrm{opt}}$) and optimal coupling

Optics EXPRESS

($\rho = \rho_{\mathrm{opt}}$), so that this absolute minimal laser power can be calculated as

$$P_{\mathrm{L,min}} = \frac{\Upsilon(\alpha_{\mathrm{opt}}, \rho_{\mathrm{opt}})}{G_{\mathrm{L,opt}}} \simeq \Upsilon\left(\pm 1, \frac{1}{2}\right) \simeq \hbar\omega_{\mathrm{L}} \frac{4\mu\kappa_{\mathrm{i}}}{g\eta} \simeq \frac{\omega_{\mathrm{L}}\Omega_{\mathrm{R}}}{gSQ_{\mathrm{i}}}\sqrt{\frac{\hbar R_{\mathrm{out}}}{Q_{\mathrm{M}}}}. \tag{53}$$

For our parameters, this value is corresponds to 4.4 mW. The reader can also note that the last approximations in Eq. (53) can be readily obtained from Eq. (51) by setting $\Gamma_{\mathrm{min}} = 1$ and extracting the equivalent optical power. It should be noted that if amplifierless miniature OEOs have the great advantage to simplify the architecture of the system, they require a careful management of the thermal effects induced in the WGM resonator by the higher laser power [45–47].

7. Conclusion

In this article, we have proposed a mathematical framework to study the time-domain nonlinear dynamics of miniature OEOs based on nonlinear WGM resonators. Our model uses time-domain equations to track the dynamics of the complex-valued envelopes of the optical and microwave fields. We have performed a stability analysis that permitted to calculate analytically the threshold value of the feedback gain that is needed to self-start the microwave oscillations. An optimization analysis has also been performed, and led us to the conclusion that the system should ideally be operated at the edge of the optical resonance and close to critical coupling. Further investigation has shown that beyond a certain laser power, RF amplification is not needed anymore and the miniature OEO can become amplifierless.

Several open points remain with regard to technology related to miniature OEOs. The first one is to understand the detrimental role played by dispersion, parasitic nonlinearities and thermal effects inside the WGM resonator [10,48]. The second challenge is to understand how the various sources of noise are translated to phase noise in the output RF signal. Modifications of the fundamental architecture can also be considered in order to achieve higher operating frequencies, such as multiple-FSR microwave pumping or frequency multiplication, for example. Finally, these miniature OEOs could also emerge as a technological platform of choice to explore several applications in quantum photonics [38,49–53].

Funding

University of Maryland (Minta Martin Fellowship).

Disclosures

The authors declare no conflicts of interest.

References

1. Y. K. Chembo, D. Brunner, M. Jacquot, and L. Larger, "Optoelectronic oscillators with time-delayed feedback," Rev. Mod. Phys. **91**(3), 035006 (2019).
2. X. S. Yao and L. Maleki, "High frequency optical subcarrier generator," Electron. Lett. **30**(18), 1525–1526 (1994).
3. X. S. Yao and L. Maleki, "Optoelectronic oscillator for photonic systems," IEEE J. Quantum Electron. **32**(7), 1141–1149 (1996).
4. X. S. Yao and L. Maleki, "Optoelectronic microwave oscillator," J. Opt. Soc. Am. B **13**(8), 1725–1735 (1996).
5. D. Eliyahu, D. Seidel, and L. Maleki, "Phase noise of a high performance OEO and an ultra low noise floor cross-correlation microwave photonic homodyne system," *IEEE Int. Freq. Contr. Symp.*, 811–814 (2008).
6. A. Matsko, A. Savchenkov, D. Strekalov, V. Ilchenko, and L. Maleki, "Review of applications of whispering-gallery mode resonators in photonics and nonlinear optics," IPN Prog. Rep. **42**, 1–51 (2005).
7. A. Chiasera, Y. Dumeige, P. Feron, M. Ferrari, Y. Jestin, G. N. Conti, S. Pelli, S. Soria, and G. C. Righini, "Spherical whispering-gallery-mode microresonators," Laser Photonics Rev. **4**(3), 457–482 (2010).
8. A. Coillet, R. Henriet, K. P. Huy, M. Jacquot, L. Furfaro, I. Balakireva, L. Larger, and Y. K. Chembo, "Microwave photonics systems based on whispering-gallery-mode resonators," J. Vis. Exp. **78**, 50423 (2013).

Optics EXPRESS

9. D. V. Strekalov, C. Marquardt, A. B. Matsko, H. G. L. Schwefel, and G. Leuchs, "Nonlinear and quantum optics with whispering gallery resonators," J. Opt. **18**(12), 123002 (2016).
10. G. Lin, A. Coillet, and Y. K. Chembo, "Nonlinear photonics with high-Q whispering-gallery-mode resonators," Adv. Opt. Photonics **9**(4), 828–890 (2017).
11. S. Fujii, Y. Hayama, K. Imamura, H. Kumazaki, Y. Kakinuma, and T. Tanabe, "All-precision-machining fabrication of ultrahigh-Q crystalline optical microresonators," Optica **7**(6), 694–701 (2020).
12. K. Volyanskiy, P. Salzenstein, H. Tavernier, M. Pogurmirskiy, Y. K. Chembo, and L. Larger, "Compact optoelectronic microwave oscillators using ultra-high Q whispering gallery mode disk-resonators and phase modulation," Opt. Express **18**(21), 22358–22363 (2010).
13. P.-H. Merrer, K. Saleh, O. Llopis, S. Berneschi, F. Cosi, and G. Nunzi Conti, "Characterization technique of optical whispering gallery mode resonators in the microwave frequency domain for optoelectronic oscillators," Appl. Opt. **51**(20), 4742–4748 (2012).
14. D. Eliyahu, W. Liang, E. Dale, A. A. Savchenkov, V. S. Ilchenko, A. B. Matsko, D. Seidel, and L. Maleki, "Resonant widely tunable opto-electronic oscillator," IEEE Photonics Technol. Lett. **25**(15), 1535–1538 (2013).
15. A. Coillet, R. Henriet, P. Salzenstein, K. P. Huy, L. Larger, and Y. K. Chembo, "Time-domain dynamics and stability analysis of optoelectronic oscillators based on whispering-gallery mode resonators," IEEE J. Sel. Top. Quantum Electron. **19**(5), 1–12 (2013).
16. K. Saleh, R. Henriet, S. Diallo, G. Lin, R. Martinenghi, I. V. Balakireva, P. Salzenstein, A. Coillet, and Y. K Chembo, "Phase noise performance comparison between optoelectronic oscillators based on optical delay lines and whispering gallery mode resonators," Opt. Express **22**(26), 32158–32173 (2014).
17. K. Saleh, G. Lin, and Y. K. Chembo, "Effect of laser coupling and active stabilization on the phase noise performance of optoelectronic microwave oscillators based on whispering-gallery mode resonators," IEEE Photonics J. **7**(1), 1–11 (2015).
18. R. M. Nguimdo, K. Saleh, A. Coillet, G. Lin, R. Martinenghi, and Y. K. Chembo, "Phase noise performance of optoelectronic oscillators based on whispering-gallery mode resonators," IEEE J. Quantum Electron. **51**(11), 1–8 (2015).
19. K. Saleh and Y. K. Chembo, "Phase noise performance comparison between microwaves generated with Kerr optical frequency combs and optoelectronic oscillators," Electron. Lett. **53**(4), 264–266 (2017).
20. J. Chen, Y. Zheng, C. Xue, C. Zhang, and Y. Chen, "Filtering effect of SiO2 optical waveguide ring resonator applied to optoelectronic oscillator," Opt. Express **26**(10), 12638–12647 (2018).
21. X. Jin, M. Wang, K. Wang, Y. Dong, and L. Yu, "High spectral purity electromagnetically induced transparency-based microwave optoelectronic oscillator with a quasi-cylindrical microcavity," Opt. Express **27**(1), 150–165 (2019).
22. A. B. Matsko, L. Maleki, A. A. Savchenkov, and V. S. Ilchenko, "Whispering gallery mode based optoelectronic microwave oscillator," J. Mod. Opt. **50**(15-17), 2523–2542 (2003).
23. L. Maleki, "The optoelectronic oscillator," Nat. Photonics **5**(12), 728–730 (2011).
24. P. Rabiei, W. H. Steier, C. Zhang, and L. R. Dalton, "Polymer micro-ring filters and modulators," J. Lightwave Technol. **20**(11), 1968–1975 (2002).
25. N. G. Pavlov, N. M. Kondratyev, and M. L. Gorodetsky, "Modeling the whispering gallery microresonator-based optical modulator," Appl. Opt. **54**(35), 10460–10466 (2015).
26. Y. Ehrlichman, A. Khilo, and M. A. Popovic, "Optimal design of a microring cavity optical modulator for efficient RF-to-optical conversion," Opt. Express **26**(3), 2462–2477 (2018).
27. A. Parriaux, K. Hammani, and G. Millot, "Electro-optic frequency combs," Adv. Opt. Photonics **12**(1), 223–287 (2020).
28. V. S. Ilchenko, A. A. Savchenkov, A. B. Matsko, and L. Maleki, "Whispering-gallery-mode electro-optic modulator and photonic microwave receiver," J. Opt. Soc. Am. B **20**(2), 333–342 (2003).
29. D. A. Cohen and A. F. J. Levi, "Microphotonic millimetre-wave receiver architecture," Electron. Lett. **37**(1), 37–39 (2001).
30. V. S. Ilchenko, A. A. Savchenkov, A. B. Matsko, and L. Maleki, "Sub-microwatt photonic microwave receiver," IEEE Photonics Technol. Lett. **14**(11), 1602–1604 (2002).
31. M. Hossein-Zadeh and A. F. J. Levi, "14.6-GHz LiNbO3 Microdisk photonic self-homodyne RF receiver," IEEE Trans. Microw. Theory Techn. **54**(2), 821–831 (2006).
32. V. S. Ilchenko, A. B. Matsko, I. Solomatine, A. A. Savchenkov, D. Seidel, and L. Maleki, "Ka-Band All-resonant photonic microwave receiver," IEEE Photonics Technol. Lett. **20**(19), 1600–1612 (2008).
33. A. B. Matsko, D. V. Strekalov, and N. Yu, "Sensitivity of terahertz photonic receivers," Phys. Rev. A **77**(4), 043812 (2008).
34. D. V. Strekalov, A. A. Savchenkov, A. B. Matsko, and N. Yu, "Efficient upconversion of subterahertz radiation in a high-Q whispering gallery resonator," Opt. Lett. **34**(6), 713–715 (2009).
35. D. V. Strekalov, H. G. L. Schwefel, A. A. Savchenkov, A. B. Matsko, L. J. Wang, and N. Yu, "Microwave whispering-gallery resonator for efficient optical up-conversion," Phys. Rev. A **80**(3), 033810 (2009).
36. A. A. Savchenkov, A. B. Matsko, W. Liang, V. S. Ilchenko, D. Seidel, and L. Maleki, "Single-sideband electro-optical modulator and tunable microwave photonic receiver," IEEE Trans. Microw. Theory Techn. **58**(11), 3167–3174 (2010).

Optics EXPRESS

37. G. S. Botello, F. Sedlmeir, A. Rueda, K. A. Abdalmalak, E. R. Brown, G. Leuchs, S. Preu, D. Segovia-Vargas, D. V. Strekalov, L. E. G. Munoz, and H. G. L. Schwefel, "Sensitivity limits of millimeter-wave photonic radiometers based on efficient electro-optic upconverters," Optica **5**(10), 1210–1219 (2018).
38. A. Rueda, F. Sedlmeir, M. C. Collodo, U. Vogl, B. Stiller, G. Schunk, D. V. Strekalov, C. Marquardt, J. M. Fink, O. Painter, G. Leuchs, and H. G. L. Schwefel, "Efficient microwave to optical photon conversion: an electro-optical realization," Optica **3**(6), 597–604 (2016).
39. As a notational convention, sans serif fonts are reserved to operators. All operators are in caps, except pure cavity fields. Calligraphic fonts are reserved for semi-classical complex-valued variables, and bold fonts stand for matrices and vectors. The same terminology applies to photon numbers.
40. Y. K. Chembo, L. Larger, R. Bendoula, and P. Colet, "Effects of gain and bandwidth on the multimode behavior of optoelectronic microwave oscillators," Opt. Express **16**(12), 9067–9072 (2008).
41. S. Diallo and Y. K. Chembo, "Optimization of primary Kerr optical frequency combs for tunable microwave generation," Opt. Lett. **42**(18), 3522–3525 (2017).
42. Y. K. Chembo, "Quantum dynamics of Kerr optical frequency combs below and above threshold: Spontaneous four-wave mixing, entanglement, and squeezed states of light," Phys. Rev. A **93**(3), 033820 (2016).
43. V. S. Ilchenko, J. Byrd, A. A. Savchenkov, A. B. Matsko, D. Seidel, and L. Maleki, "Miniature oscillators based on optical whispering gallery mode resonators," *Proc. IEEE Intl. Freq. Cont. Symp.*, 305–308 (2008).
44. W. Loh, S. Yegnanarayanan, J. Klamkin, S. M. Duff, J. J. Plant, F. J. O'Donnell, and P. W. Juodawlkis, "Amplifier-free slabcoupled optical waveguide optoelectronic oscillator systems," Opt. Express **20**(17), 19589–19598 (2012).
45. Y. Deng, R. Flores-Flores, R. K. Jain, and M. Hossein-Zadeh, "Thermo-optomechanical oscillations in high-Q ZBLAN microspheres," Opt. Lett. **38**(21), 4413–4416 (2013).
46. S. Diallo, G. Lin, and Y. K. Chembo, "Giant thermo-optical relaxation oscillations in millimeter-size whispering gallery mode disk resonators," Opt. Lett. **40**(16), 3834–3837 (2015).
47. Y. Pan, G. Lin, S. Diallo, X. Zhang, and Y. K. Chembo, "Design of X-cut and Z-cut lithium niobate whispering-gallery-mode disk-resonators with high quality factors," IEEE Photonics J. **9**(4), 1–8 (2017).
48. G. Lin, S. Diallo, J. M. Dudley, and Y. K. Chembo, "Universal nonlinear scattering in ultra-high Q whispering gallery-mode resonators," Opt. Express **24**(13), 14880–14894 (2016).
49. D. V. Strekalov, A .A. Savchenkov, A. B. Matsko, and N. Yu, "Towards counting microwave photons at room temperature," Laser Phys. Lett. **6**(2), 129–134 (2009).
50. M. Tsang, "Cavity quantum electro-optics," Phys. Rev. A **81**(6), 063837 (2010).
51. M. Tsang, "Cavity quantum electro-optics. II. Input-output relations between traveling optical and microwave fields," Phys. Rev. A **84**(4), 043845 (2011).
52. S. Huang, "Quantum state transfer in cavity electro-optic modulators," Phys. Rev. A **92**(4), 043845 (2015).
53. A. M. Hagerstrom, T. E. Murphy, and R. Roy, "Harvesting entropy and quantifying the transition from noise to chaos in a photon-counting feedback loop," Proc. Natl. Acad. Sci. **112**(30), 9258–9263 (2015).